Electronic Supplementary Material (ESI) for Chemical Communications.
This journal is © The Royal Society of Chemistry 2021

Electronic Supplementary Information

Plasmonic nanorod array for effective photothermal therapy in hyperthermia

Thanh Lam Bui, [†a] Ngoc Thanh Ho, [†a] Xuan Vuong Thi Thanh Ho,[a] Dinh Nghi Ngo,[a] Soon Hyuk Lim,[b] Sang Jun Son,*[b] Seung Man Noh, *[c] Sang-Woo Joo*[a]

[a] Department of Information Communication, Materials, and Chemistry Convergence Technology, Soongsil University, Seoul 06978, Republic of Korea. Email: sjoo@ssu.ac.kr

[b] Department of Chemistry, Gachon University, Seongnam 13120, Republic of Korea. Email: sjson@ganchon.ac.kr

[c] Research Center for Green Fine Chemicals, Korea Research Institute of Chemical Technology, Ulsan 681-310, Republic of Korea. Email: smnoh@krict.re.kr

[†] These authors contributed equally to this work.

Experimental Section

Materials

Aurochloric acid ($HAuCl_4$), hexadecyltrimethylammonium bromide (CTAB), L-ascorbic acid ($C_6H_8O_6$), methoxypolyethylene glycol thiol (PEG-SH 5000), sodium borohydride ($NaBH_4$), rhodamine 6G (R6G), silver nitrate ($AgNO_3$), and trypan blue were acquired from Sigma–Aldrich. Toluene, Oxalic acid, chromic acid, tetrahydrofuran (THF), perchloric acid, and phosphoric acid were purchased from Daejung. Aluminum foils were used from Alfa Aesar. Dulbecco's modification of Eagle's medium (DMEM, Welgene-Daegu, Korea), Roswell Park Memorial Institute 1640 media (RPMI 1640, Welgene-Daegu, Korea), Fetal Bovine Serum (FBS, Welgene-Daegu, Korea), Dulbecco's Phosphate-Buffered Saline (DPBS, Welgene-Daegu, Korea) buffer, penicillin-streptomycin solution (100×) was purchased from Gen Depot (Barker, USA), HeLa cells line were taken from Korean cell line bank.

Synthesis of AuNRs

The minor modification seed mediated method from El-Sayed and his co-worker was used to synthesize AuNRs.[S1] To prepare the gold seeds solution, an ice-cold $NaBH_4$ solution (60 μL of 100 mM) was dropped to the solution containing the CTAB (10 mL of 100 mM), $HAuCl_4$ (200 μL of 25 mM) under vigorously stirring. The prepared seed mixture was kept undisturbed under 25 °C for 24 h. The preparation of the growth solution including the addition of $HAuCl_4$ (200 μL of 25 mM), $AgNO_3$ (150 μL of 3.1 mM), and ascorbic acid solution (150 μL, 38 mM) to CTAB solution (0.1 M, 10 mL). Then, in the growth solution, an amount of the seed solution was introduced and kept under room temperature overnight. To reduce the excessive CTAB ligand, AuNRs were collected at 5000 rpm for 5 min and the precipitate was dissolved into purify water for further purification.

AAO Template Preparation

AAO fabrication is described in our work consisting of two-step anodization. The electropolishing step was performed in a solution containing C_2H_5OH and $HClO_4$ (5:1, volume) to reduce roughness on the surface of as-annealed aluminum foils (3x10 cm). After pretreatment, the first anodization was conducted at the current 40 V (10 °C) for 7 h in 300 nM oxalic acid solution. The next step was to remove the resultant aluminum oxide by emerging the substrate in aqueous H_3PO_4 acid and H_2CrO_4 acid at 6 and 1.8 wt% respectively, for 270 min at 60 °C. Then the second anodization was performed with the same condition from the previous one to control the depth of the pore. Finally, the pore diameter was adjusted by the etching process in H_3PO_4 acid (5 wt%, 30 °C).

PEG-SH Modification

The CTAB ligand on the surface of AuNRs was eliminated by PEG-SH (5000).[S2,3] In brief, an amount of PEG-SH solution (0.5 mL, 4 mM) was introduced to the purified AuNRs with vigorous stirring. The mixture was left stirring for 24 h, then the centrifugation was performed (5000 rpm, 5 min), and resuspended the precipitate in THF. Then, the amount of ethanolic solution of PEG-SH was added under gently stirring in 24 h. Finally, the centrifugation was repeated one time and the purified AuNR solution was dispersed in 5 mL of toluene.

Ultrasonication-assisted AuNR array

The ultrasonic technique was applied to fabricate the AuNRs@AAO array. Firstly, the ordered porous AAO template with the dimension 2x0.5 cm was put into the Eppendorf containing the purified AuNRs solution and then immerged in the ultrasonic bath with the desirable time at 25 °C. The template was sonicated in another Eppendorf containing pure toluene to remove the excess AuNRs bounding on the

surface. The process above should be repeated 3 times to ensure that all the AAO nanopore obtain internally monomeric of AuNRs.
Using this methodology, the array of metallic nanoparticles in large areas of up to centimeter square is feasible without any complex instruments. Our approach is advantageous in comparison with conventional lithographic techniques or droplet evaporation. In principle, the combination of the excellent dimensions of AuNRs and AAO nanopore is an important factor for introducing a single nanorod in every nanopore (Scheme 1B).[S4] The length and width of AuNRs were adjusted when changing the amount of Au seed solution or $AgNO_3$ concentration. The dimensions of the AAO nanopore were manipulated by the time of the second anodization and pore widening step. The length of the AAO nanopores in all three templates was nearly consistent with 60 s of anodization.
The ultrasonication-assisted self-assembly process was accomplished with good uniformity over large areas (Fig. 1, S1, S7). Therefore, AuNRs can introduce smoothly to AAO nanopore in a hydrophobic solvent. Unattached AuNRs at the orifice can be removed by rinsing several times in an ultrasonic bath. By taking advantage of the AAO template, the self-assembly takes place to design a unique structure that can be utilized for functional device applications. It is necessary to isolate nanoparticles to study the fundamental properties of a noble metallic nanostructure. In addition to the rod shape, this method can be applied for different morphologies that are without aggregation or that have irregular structures.

Plasma Treatment

For R6G SERS measurement, the AuNRs@AAO substrate was cleaned under plasma treatment to remove the ligand on the surface of the AuNRs@AAO. The substrates were placed in the plasma chamber with 25 sccm of Argon gas, 40 W, and process was completed in 40 s.

Cell Culture on Bare AAO and AuNRs@AAO Substrates

DMEM and RPMI 1640 media after being treated with a solution of 1 % penicillin-streptomycin and 10 % FBS (100X) at 37 °C, were kept at 4 °C before warming up to 37 °C for HeLa cell culture. Bare AAO, AuNRs@AAO substrates were firstly sterilized by ethanol before growing on its surface. The normal cells detached by trypsin were cultured in 96-well plate containing bare AAO, AuNRs@AAO substrates. The density of cells on AAO was approximately controlled at $2x10^5$ cells cm^{-2} and maintained in the incubator at 37 °C for 48 h.

Thermographic Images, Photothermal Therapy, and Fluorescence Images

The AAO, AuNRs@AAO substrates (4x4 mm) covered by a monolayer of cells were taken out of the 96-well plate and rinsed with DPBS buffer. Then, the cancerous cell on the surface substrates was covered by a few microliters of media and exposed under 671 nm laser (2 mm diameter of the beam) in 5 minutes. The thermographic images were taken by the thermal camera (FLIR C2), object temperature range from −10 °C to 150 °C. After 5 minutes of laser exposure, the system was stained, incubated with Trypan Blue for 10 minutes per sample. The samples after being stained were perceived under the optical microscope (10x objective lens) in the bright field. The fluorescence images of damaged cells stained with trypan blue on substrates were observed under the Olympus IX-71 inverted microscope integrated with a Coolsnap HQ CCD camera and a 10X objective lens and. The excitation filter 607AF75, emission filter 695AF55, and dichroic XF2019 were used to obtain the fluorescence images. All images were captured and analyzed by MetaMorph software.

COMSOL Simulation

The absorption spectra and electric field enhancement of AuNRs were calculated using the package of COMSOL Multiphysics Version 5.3a. The sizes of AuNRs were chosen to be 69 and 32 nm respectively to the length and the width. In our model, the Au and

Al_2O_3 permittivity were taken from the data measured by Johnson and Christy, and Hagemann respectively. The electric field was along to the x axis and the incident light was along with the z axis. The AuNRs@AAO substrate was introduced into the middle of an air spherical domain (∅= 2 μm) to avoid reflection by a perfectly matched layer boundary condition. In every structure, as with the P6 model, although the simulation was expanded up to 127 AuNRs@AAO nanopore, the $|E/E_0|$ number was nearly constant, with only slight fluctuations. Similar results were also observed with the P8 and P10 structures (Table S3). Remarkably, the tilted AuNRs were encapsulated into isolated nanopore that successfully confirmed the well-qualified shape of the template.

The local electric field computations of up to 127 AuNRs@AAO nanopores in three substrates were conducted to clarify whether the adjacent AuNRs@AAO nanopore exhibited plasmonic coupling and amplified the longitudinal intensity (Fig. S5D-F, S8-S10). The tilted angle of AuNR in P6, P8, and P10 substrates was hypothesized as 6, 8, and 12 degrees. The junction between nanoparticles was dependent on their nanogap distance. In our work, the AuNR–AuNR distance was estimated through the edge-to-edge distance of AAO nanopore. These parameters were 70.8 nm, 66.9 nm, and 63.6 nm following pore widening of 6, 8, and 10 min for P6, P8, and P10 substrates, respectively (Table S2). As the result, an increase in the tilted angle of AuNR when expanding nanopore caused mainly an outstanding enhancement of the electric field. The $|E/E_0|$ values of P6, P8, and P10 of single AuNRs@AAO nanopore were 7.89, 11.51, and 14.75, respectively. Because the distance between AuNRs was greater than 60 nm, the interaction of adjacent AuNRs can be practically negligible. The plasmonic coupling dependent on the distance of Au nanoparticles was demonstrated in previous research.[S5]

Considering that electromagnetic enhancements vary with the cos2(q).[S6] As indicated in Fig. S5A, B, C and Fig. S7D, the absorbance increases of the longitudinal modes and the consequent SERS intensities indicate that our experimental data would be in an agreement with the theoretical considerations.

According to the Clausius-Mossotti equation, the transverse and longitudinal modes can be express as:[S7, 8]

$$\alpha_j = \frac{4\pi ab^2}{3P_j} \frac{\varepsilon - \varepsilon_m}{\varepsilon + \left(\frac{1-Pj}{Pj}\right)\varepsilon_m}$$

where a and b are the length and the width of AuNR particles; ε and ε_m are the dielectric constant of the AuNR particle and surrounding medium; j is the longitudinal and transverse modes; and P_j is the depolarization factor.

The relative absorbance changes can be explained by the polarizability changes:[S7]

$$C_{abs} = k\, Im(\alpha)$$

In every structure, as with the P6 model, although the simulation was expanded up to 127 AuNRs@AAO nanopore, the |E/E0| number was nearly constant, with only slight fluctuations. Similar results were also observed with the P8 and P10 structures (Table S3). Remarkably, the tilted AuNRs were encapsulated into isolated nanopore that successfully confirmed the well-qualified shape of the template.

Characterization

TEM images of AuNRs particle were characterized by a JEM-2100 electron microscope (JEOL Co., Ltd, Japan). A JEM-ARM200F electron microscope equipped with a cold FEG was operated to observe the HAADF-STEM atomic resolution of AuNR particles (JEOL

Co., Ltd, Japan). SEM images of AuNRs@AAO substrates were obtained in a field emission Zeiss Gemini 300 (Carl Zeiss Microscopy, Germany). AFM images were acquired from ezAFM+ system (Nanomagnetic Instruments, UK). UV-Vis absorption spectroscopy of AuNR solution and monomeric AuNRs@AAO arrays were obtained in an Optizen 3220UV (Mecasys Co., Ltd, South Korea), and a UV-3600 Shimadzu spectrophotometer (Shimadzu Corporation, Japan), respectively. A zeta potential analyzer (ELSZ-2000 series, Otsuka Electronics Co., Ltd. Japan) was used to calculate the AuNR particles' zeta potential values. To collect the infrared spectra, a PIKE technology ATR-IR accessory (Nicolet 6700 FT-IR, Thermo Scientific Inc, USA) was operated and the spectrum was then deconvoluted by a Systat PeakFit software program. A VITA (Femtoscience Inc, South Korea) plasma etching system was used for plasma treatment. Ultrasonic procedures were carried out on the ultrasonic bath (SD-200H/40kHz – Shin Jin Corp., South Korea). In the photothermal therapy experiments, a 671 nm red laser having a beam diameter of 2.0 mm at the aperture and a divergence of lower than 1.5 mRad (model SDL-671-XXXT, Shanghai Dream Lasers Technology Co., Ltd., Chinca) was used. An Ophir power meter (Vega P/N 7Z01560, Ophir, Israel) was employed to measure the laser power.

Renishaw research laser Raman spectroscopy microscope (RM1000) was operated to obtain SERS spectra (633 nm laser, 25 LHP 928, Melles Griot, USA). R6G was chosen as a probe to verify the SERS efficiency and sensitivity of the AuNRs@AAO substrate. As shown in Fig. S7A, the Raman peaks at 610 cm^{-1} (C–C–C ring in-plane bending), 771 cm^{-1} (out-of-plane bending), and 1180, 1308, 1357, 1505 and 1648 cm^{-1} (C-C stretching) in the SERS spectrum were consistent with the previous report for R6G.[S8] This demonstrates that our substrates acquired outstanding SERS activity. All vibrations were strongly enhanced in SERS measurement, whereas a few peaks appeared in the normal Raman spectrum. By utilizing the P10 substrate, SERS spectra measurements of R6G molecules on the substrate with various concentrations from 1 µM to 1 nM were investigated. The intensity reduced when the concentration of R6G decreased. The limit of detection (LOD) for R6G is 1 nM, as evidenced by the peaks at 610, 771, 1357, 1505, and 1648 cm^{-1} on the P10 substrate. In addition to the sensitivity of the substrate, the SERS spectra and intensity of R6G (5 nM) on AuNRs@AAO from 15 randomly selected points were obtained to confirm the regularity and reproducibility (Fig. S7B, C).

It is thus acceptable to conclude there is the excellent reproducibility of the AuNRs@AAO for sensing applications and photothermal therapy. Furthermore, the SERS performances of R6G on three different AuNRs@AAO substrates (P6, P8, and P10) were obtained and compared with each other (Fig. S7D). The intensities of the peak at 610 cm^{-1} were ~5234, ~9486, ~22127 a.u. for P6, P8, P10 substrates, respectively. Obviously, among the three different substrates, the SERS signal was most significantly enhanced on the P10 substrate.

The interpretation for enhancement of the AuNR array is related to the dependence of the shape of a metal nanostructure on the electromagnetic field. This is the so-called lightning rod effect.[S9] The lightning rod effect causes the electric field near the curved surface to be stronger with greater curvatures. The SERS enhancement factor was strongly related to the local electric field of nanomaterial (E_{loc}) over the incident field (E_0) in different frequencies (w_0, w_R) at position r_m which could be approximately calculated with the following equation:[S10]

$$EF(\omega_0, \omega_R, r_m) \approx \left|\frac{E_{loc}(\omega_0, r_m)}{E_0(\omega_0, r_m)}\right|_2 . \left|\frac{E_{loc}(\omega_R, r_m)}{E_0(\omega_R, r_m)}\right|^2 \approx \left|\frac{E_{loc}(\omega_0, r_m)}{E_0(\omega_0, r_m)}\right|^4$$

In our work, the results emphasized that the SERS enhancement was significantly increased when the pore diameter was enlarged to induce the greater tilt angle of AuNRs.

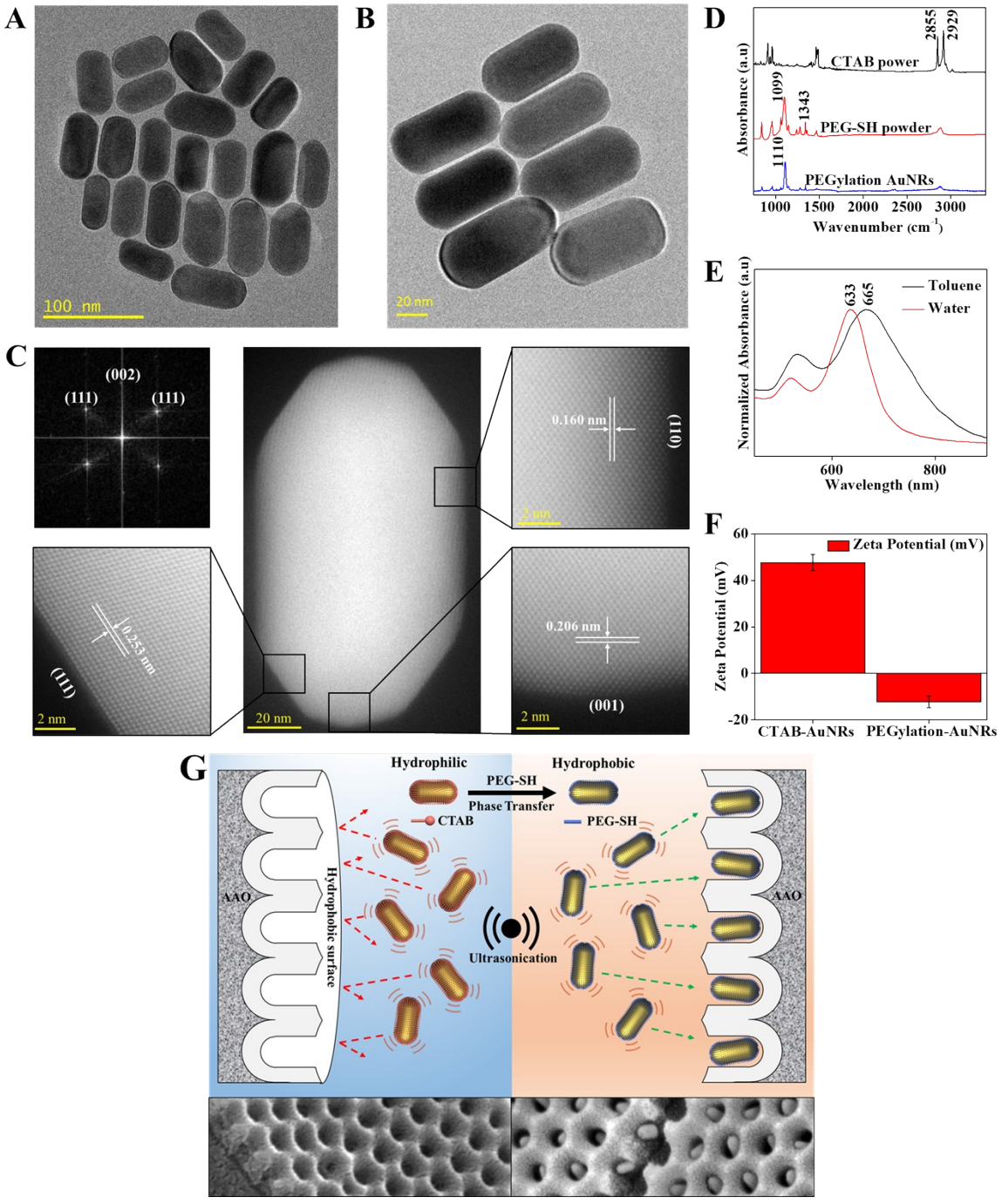

Fig. S1. (A), (B) TEM images of AuNRs in water and toluene. (C) HAADF-STEM and FFT images of single AuNRs. (D) FT-IR spectra of CTAB, PEG-SH powders, and PEGylated AuNRs. Compared with the FT-IR spectra of CTAB and PEG-SH powders as a reference, the PEGylation AuNR spectrum indicated a band for PEG-SH at 1110 cm^{-1}, in the absence of CTAB peaks at 2855 and 2929 cm^{-1}, which strongly supports the success of the PEGylation. (E) UV-Vis spectra of AuNRs in water (red curve) and toluene (black curve). (F) Zeta potential measurements of AuNRs before and after PEGylation. (G) Ultrasonication assembly scheme.

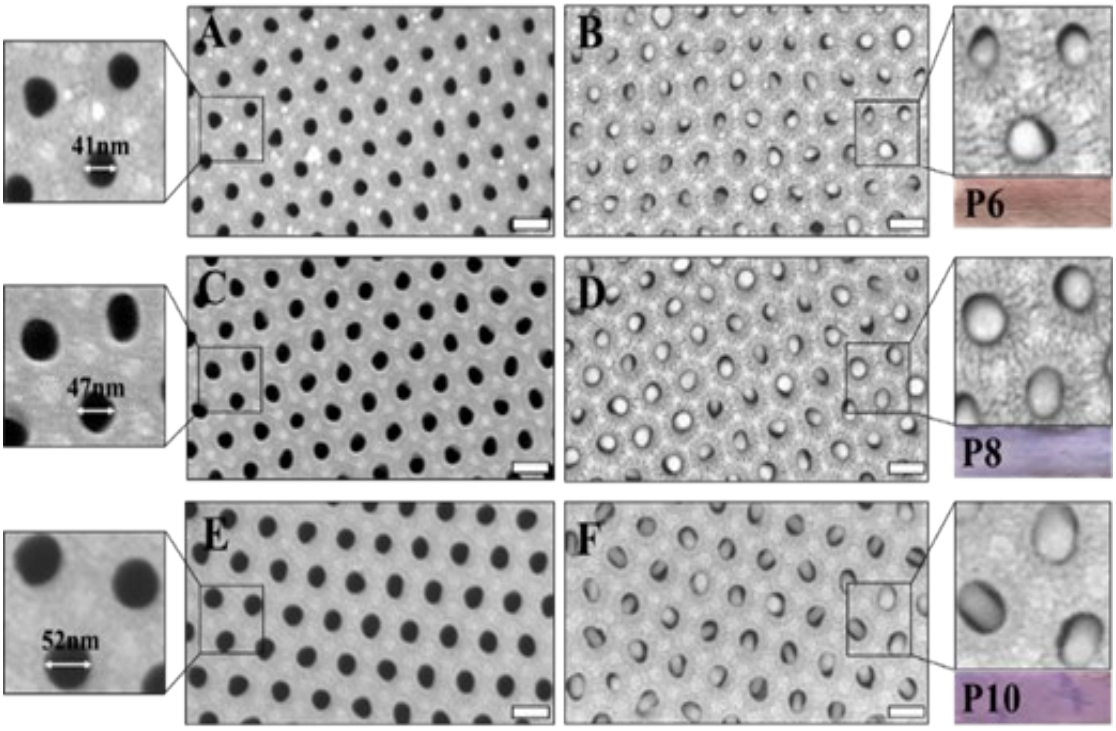

Fig. S2. (A), (C), (E) SEM images of bare AAO with 6, 8, 10 min pore-widening. (B), (D), (F) SEM images of monomeric AuNR array from the top view and the visual color of 3 different AuNRs@ AAO substrates (P6, P8, P10). All scale bars are 100 nm.

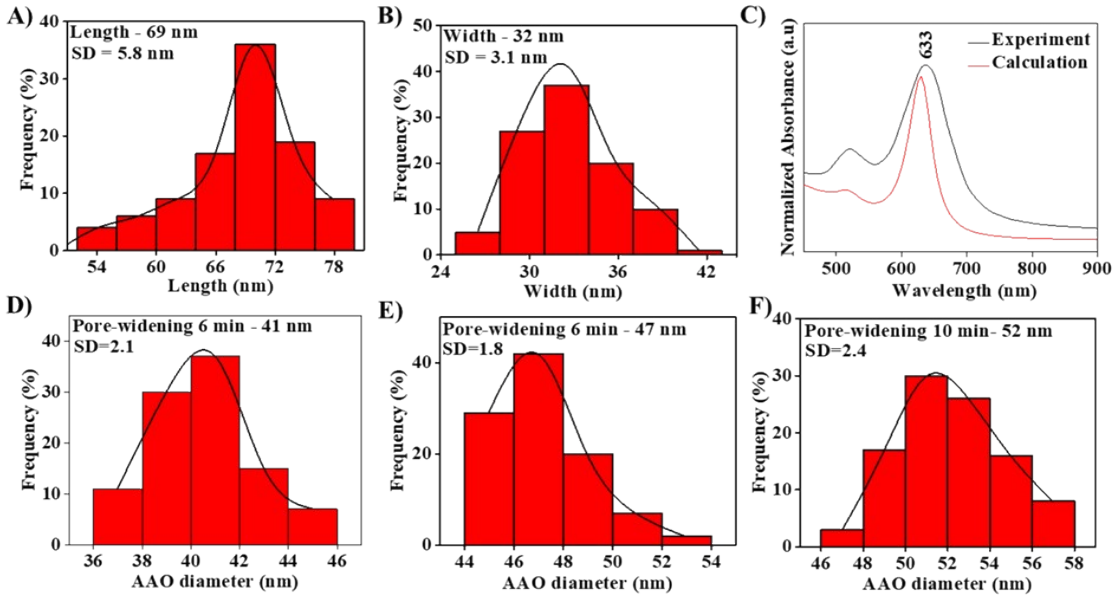

Fig. S3. (A), (B) Average length and width distributions of AuNRs. (C) Comparison of experiment and calculation UV-Vis spectra of AuNR particle in water. (D), (E), (F) Average pore distributions of bare AAO with 6, 8, 10 min pore-widening to fabricate AuNRs@AAO (P6, P8, P10) substrates

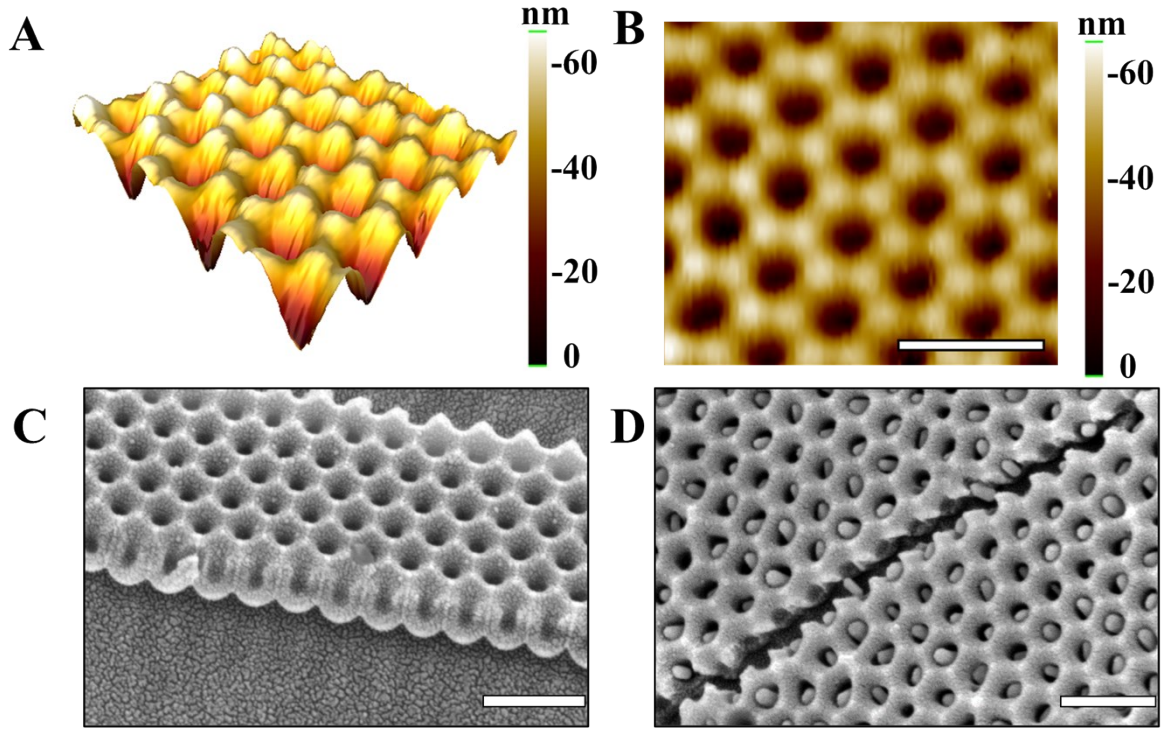

Fig S4. (A, B) AFM images of bare AAO substrate (10 min pore-widening). (C, D) Cross-section SEM images of bare AAO substrate and AuNRs@AAO nanopores (P10).

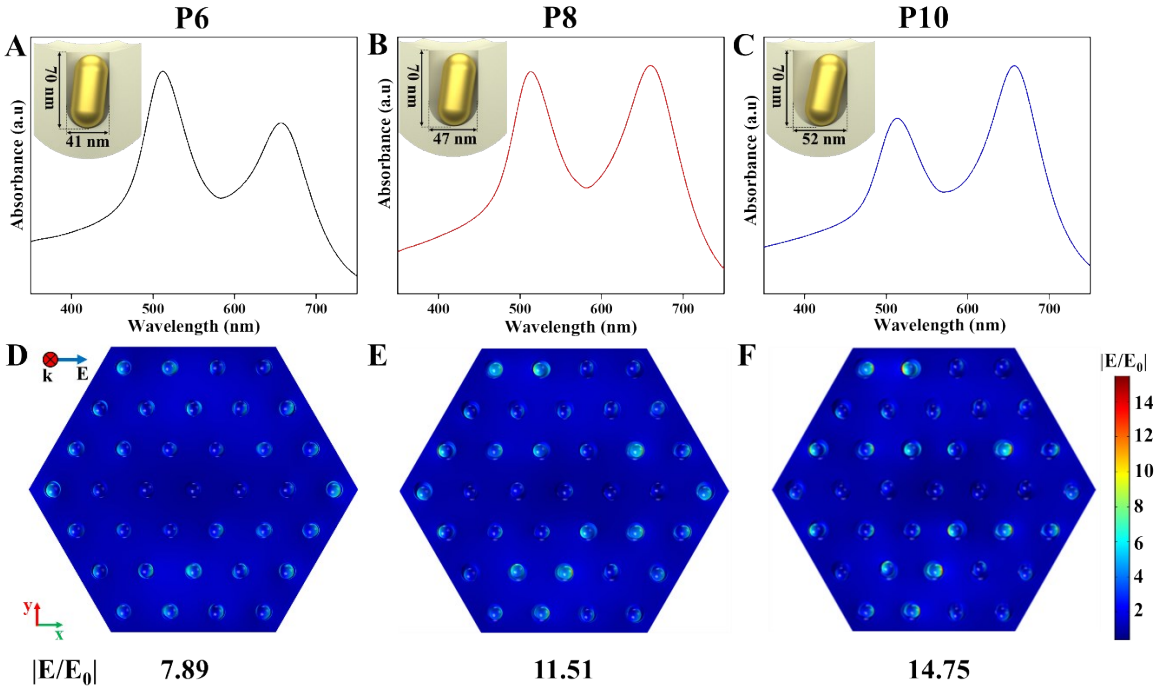

Fig. S5. (A, B, C) Experimental absorbance spectra of AuNRs@AAO substrates (P6, P8, P10). (D), (E), (F) Local electric field calculation of 37 AuNRs@AAO nanopore of P6, P8, P10.

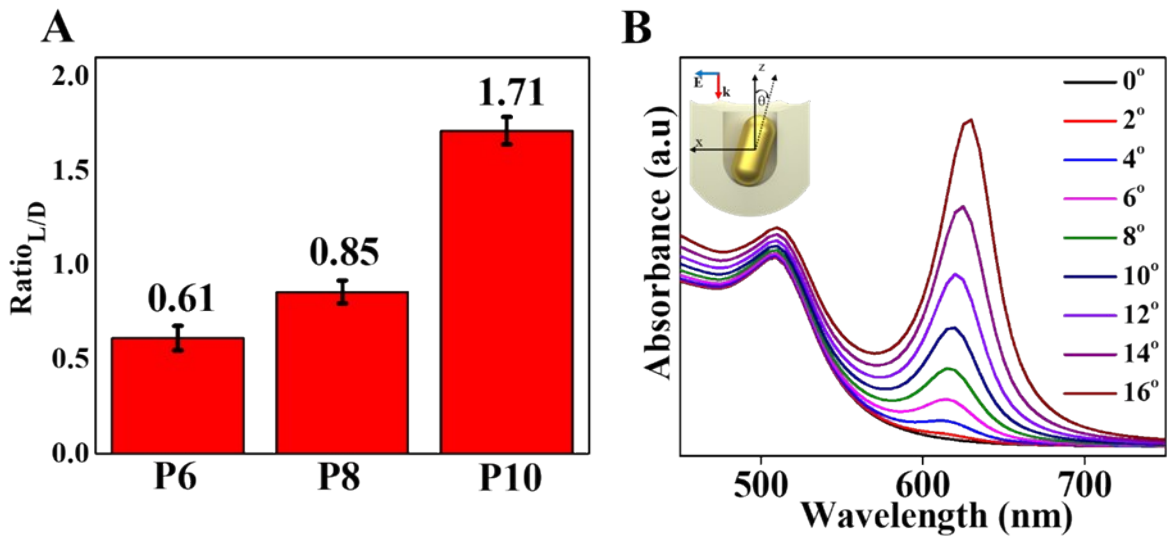

Fig. S6. (A) Ratio comparison of longitudinal intensity with respect to transverse plasmonic peak intensity. (B) Numerical calculation of AuNRs@AAO nanopore with different degrees of angles.

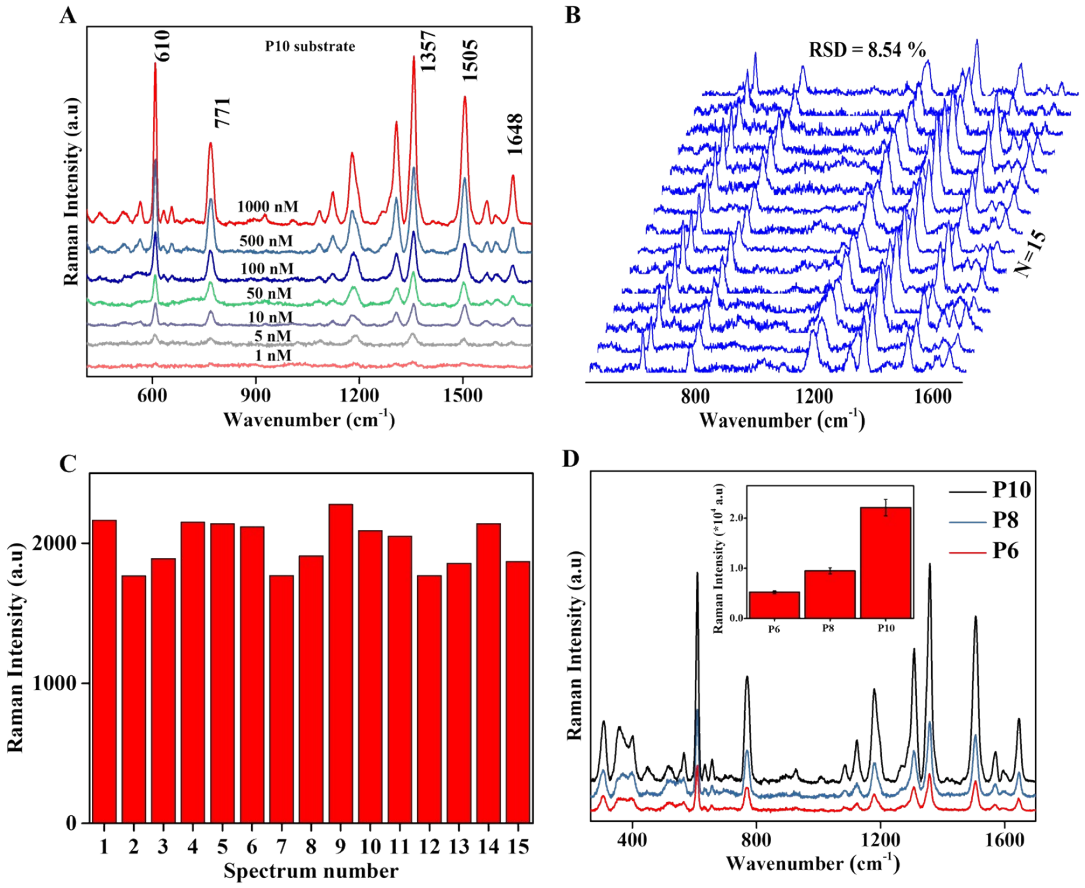

Fig. S7 (A) SERS spectra of R6G using P10 substrate with different concentrations. (B, C) SERS of R6G on AuNR array with different concentrations, and 15 randomly different points and Raman intensity at 5 nM, the spectra were collected from P10 substrate. (D) SERS spectra and Raman intensity at peak position 610 cm^{-1} of R6G on 3 different AuNRs@AAO substrates (P6, P8, P10).

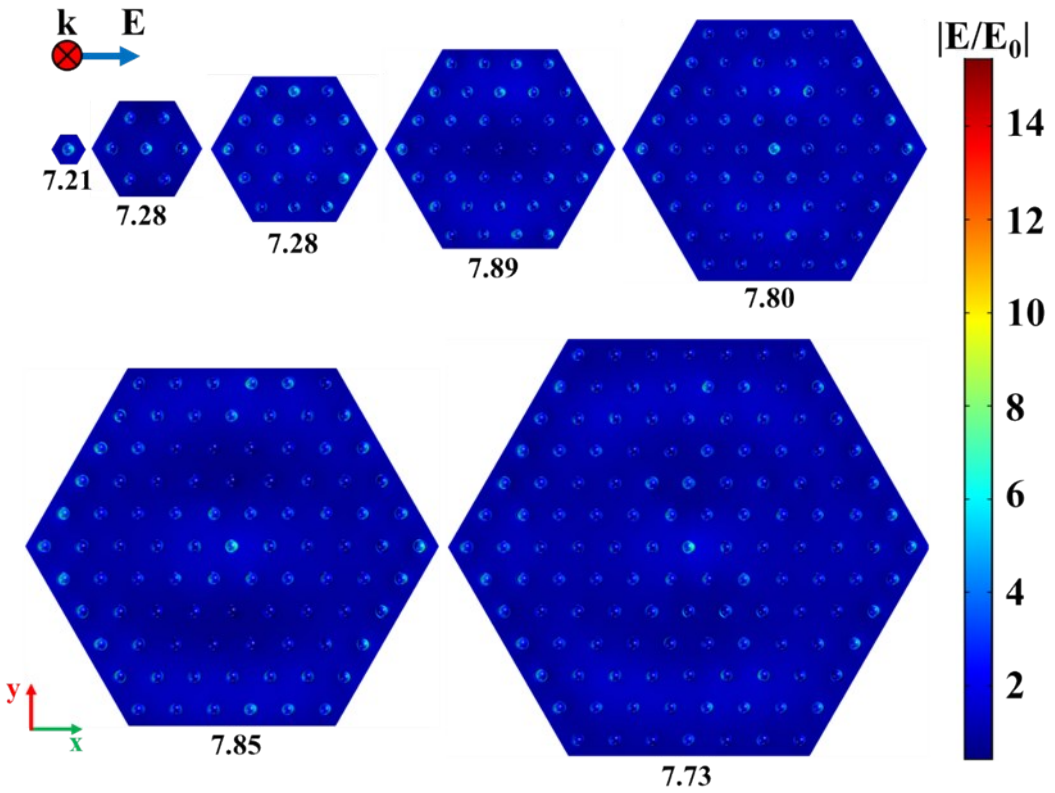

Fig. S8. Local electric field calculation of P6 structure from 1, 7, 19, 37, 61, 91, and 127 AuNRs@AAO nanopores.

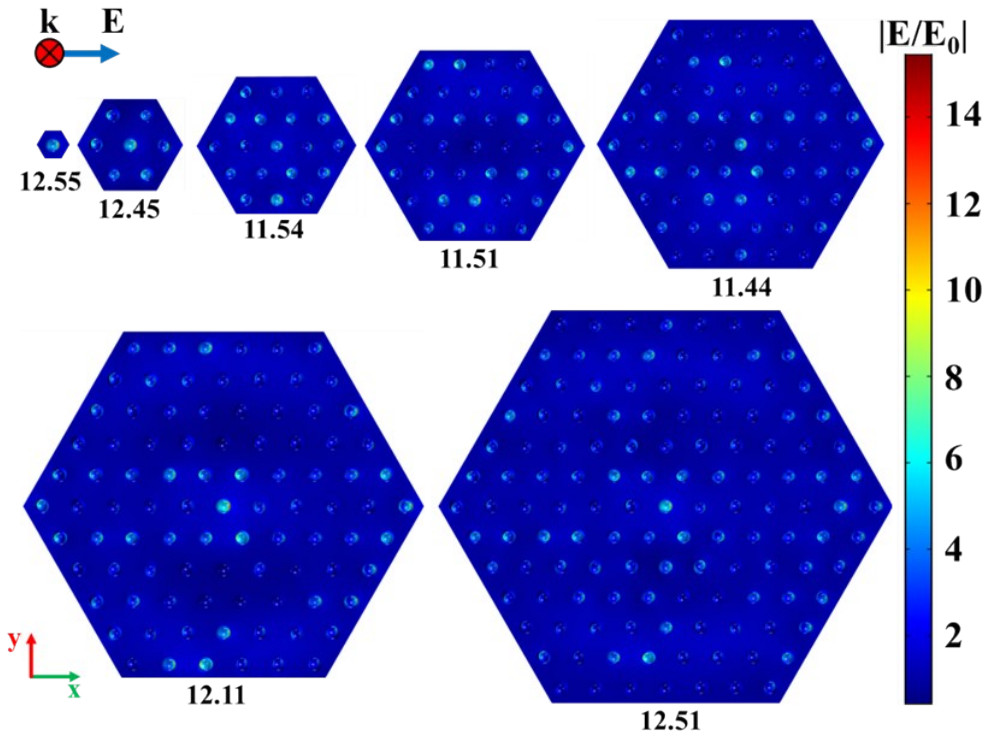

Fig. S9. Local electric field calculation of P8 structure from 1, 7, 19, 37, 61, 91, 127 AuNRs@AAO nanopores.

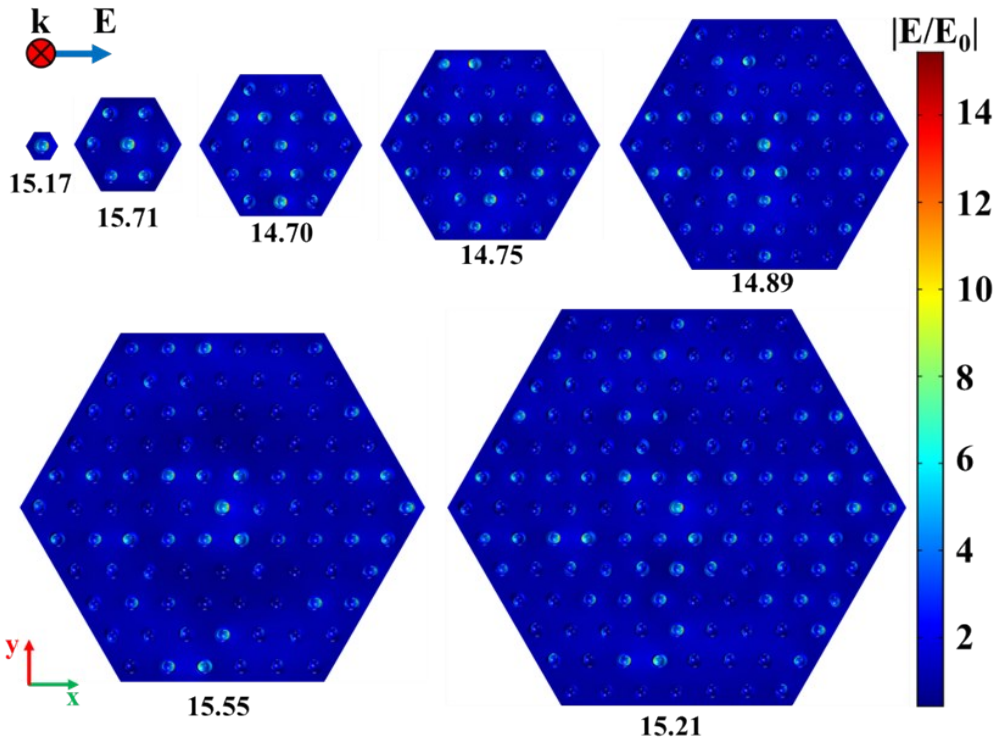

Fig. S10. Local electric field calculation of P10 structure from 1, 7, 19, 37, 61, 91, 127 AuNRs@AAO nanopores.

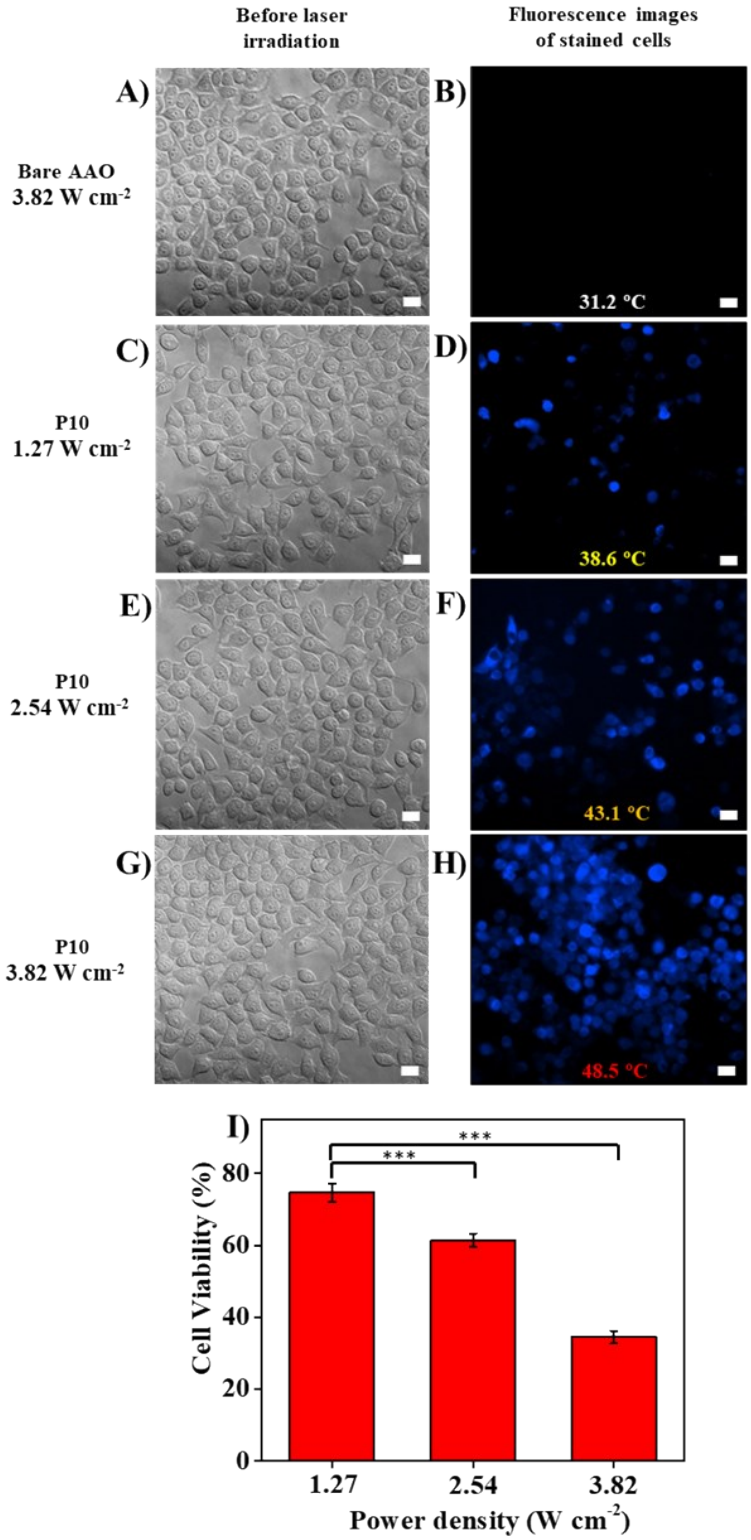

Fig. S11. (A), (C), (E), (G) Cell images of bare AAO, and P10 substrates. (B), (D), (F), (H) Fluorescence images of cancerous cell on bare AAO and P10 substrates after the laser exposure for 5 min and dying by trypan blue, (all scale bars are 50 μm). (I) Cell viability on bare AAO and P10 substrates after exposure to 671 nm laser with different laser power density from 1.27, 2.54 to 3.82 W cm^{-2} in 5 min (*: significant difference P-value < 0.05, **: highly significant difference P-value < 0.01, ***: very highly significant difference P-value < 0.001), all scale bars are 50 μm.

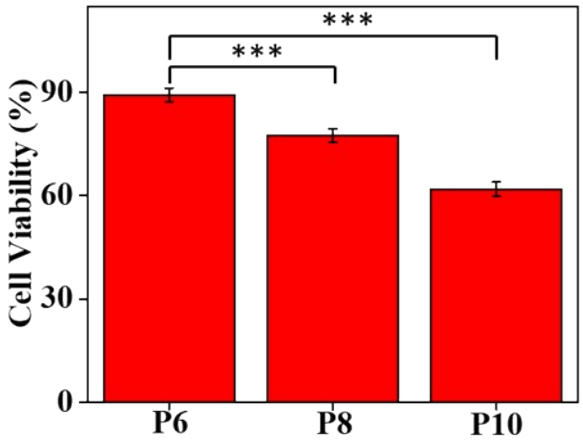

Fig. S12. Comparison of photothermal efficiency in three different AuNRs@AAO substrates (P6, P8, P10) for HeLa killing at 2.54 W cm^{-2} laser irradiation (*: significant difference P-value < 0.05, ** highly significant difference P-value < 0.01).

References

S1. B. Nikoobakht and M. A. El-Sayed, *Chem. Mater.*, 2003, **15**, 1957-1962.

S2. C. Kinnear, H. Dietsch, M. J. D. Clift, C. Endes, B. Rothen-Rutishauser and A. Petri-Fink, *Angew. Chem. Int. Ed.*, 2013, **52**, 1934-1938.

S3. B. Thierry, J. Ng, T. Krieg and H. J. Griesser, *Chem. Commun.*, 2009, 1724-1726.

S4. Y. Xia, Y. Yin, Y. Lu and J. McLellan, *Adv. Funct. Mater.*, 2003, **13**, 907-918.

S5. M. Hentschel, M. Saliba, R. Vogelgesang, H. Giessen, A. P. Alivisatos and N. Liu, *Nano Lett.*, 2010, **10**, 2721-2726.

S6. J. Wu, X. Lu, Q. Zhu, J. Zhao, Q. Shen, L. Zhan and W. Ni, *Nano-Micro Letters*, 2014, **6**, 372-380.

S7. M. Gluodenis and C. A. Foss, *J. Phys. Chem. B*, 2002, **106**, 9484-9489.

S8. L. Shao, K. C. Woo, H. Chen, Z. Jin, J. Wang and H.-Q. Lin, *ACS Nano*, 2010, **4**, 3053-3062.

S9. K. L. Kelly, E. Coronado, L. L. Zhao and G. C. Schatz, *J. Phys. Chem. B*, 2003, **107**, 668-677.

S10. S.-Y. Ding, E.-M. You, Z.-Q. Tian and M. Moskovits, *Chem. Soc. Rev.*, 2017, **46**, 4042-4076.

Table S1. Statistical distribution of the diameter *(D)*, length *(L)* of AAO; the yield *(F)* of AuNR array inside AAO substrates with different pore-widening time.

Type	D (nm)	L (nm)	F (%)
Bare AAO, pore-widening 6 min.	41 (± 2.1)	69 (± 3.8)	95.24
Bare AAO, pore-widening 8 min.	47 (± 1.8)	71 (± 4.2)	94.78
Bare AAO, pore-widening 10 min.	52 (± 2.4)	70 (± 3.4)	94.66
AuNRs	32 (± 5.8)	69 (± 3.1)	

Table S2. Statistical edge-to-edge distribution of bare AAO substrates with different pore- widening time.

Type	N (total)	Mean (nm)	SD
Bare AAO, pore-widening 6 min	100	70.8	2.5
Bare AAO, pore-widening 8 min	100	66.9	3.1
Bare AAO, pore-widening 10 min.	100	63.6	3.8

Table S3. Statistical value of $|E/E_0|$ by 3 different P6, P8, P10 substrates varying from 1 to 127 nanopores.

Sample	Number of nanopore						
	1	7	19	37	61	91	127
P6	7.21	7.28	7.28	7.89	7.8	7.85	7.73
P8	12.55	12.45	11.54	11.51	11.44	12.11	12.51
P10	15.17	15.71	14.7	14.75	14.89	15.55	15.21

Table S4. Statistical temperature value of bare AAO and P10 substrates under exposure to 671 nm laser from 1.27 to 3.82 W cm^{-2} for 5 min.

Laser power density (W cm^{-2})	Bare AAO (°C)	SD	P10 substrate (°C)	SD
1.27	28.3	1.1	38.6	2.1
2.54	29.4	1.5	43.1	2.4
3.82	31.2	1.4	48.5	2.0

Table S5. Statistical temperature value of 3 different bare AAO substrates and P6, P8, P10 samples under exposure to 671 nm laser at 2.54 W cm^{-2} for 5 min.

Type	T (°C)	SD
Bare AAO, pore-widening 6 min	28.3	2.1
Bare AAO, pore-widening 8 min	28.8	1.6
Bare AAO, pore-widening 10 min	28.6	1.5
P6 substrate	34.3	1.2
P8 substrate	37.9	1.5
P10 substrate	42.1	1.6